1 **TITLE:** Royal knifefish generate powerful suction feeding through large neurocranial elevation

2 and high epaxial muscle power

3

4 **RUNNING TITLE:** Epaxial-dominated feeding in knifefish

5

6 **KEY WORDS:**

7 XROMM, Fluoromicrometry, Muscle strain, Buccal pressure, Body shape, Buccal volume

8

9 Ellen Y. Li[1*], Elska B. Kaczmarek[1*], Aaron M. Olsen[1,2], Elizabeth L. Brainerd[1], Ariel L. Camp[1,3]

10

11 [1]Department of Ecology, Evolution and Organismal Biology, Brown University, Providence RI

12 02912; [2]3D Anatomy Studios, Providence RI; [3]Department of Musculoskeletal and Ageing

13 Science, Institute of Life Course and Medical Sciences, University of Liverpool, Liverpool L7

14 8TX, UK

15

16 *Co-first authors

17

18 **SUMMARY STATEMENT**

19 Royal knifefish rely on their distinct postcranial morphology--with a curved vertebral column

20 and large dorsal body muscles--to produce large neurocranial elevation and powerful suction

21 feeding.

22
23 Author Contributions:
24
25 Conceptualization - ALC, ELB
26 Methodology - ALC, AMO, ELB
27 Software - ALC, AMO, EBK, EYL
28 Formal Analysis - ALC, EYL
29 Investigation - ALC, AMO, EBK, EYL
30 Writing - Original Draft Preparation - EBK, ELB, EYL
31 Writing - Review & Editing - ALC, AMO, EBK, ELB, EYL
32 Visualization - ALC, EBK, EYL
33 Supervision - ALC, AOM, EBK, ELB
34 Project Administration - ELB
35 Funding Acquisition - ALC, ELB
36

37   **ABSTRACT**

38   Suction feeding in ray-finned fishes involves powerful buccal cavity expansion to

39   accelerate water and food into the mouth. Previous XROMM studies in largemouth bass

40   (*Micropterus salmoides*), bluegill sunfish (*Lepomis macrochirus*), and channel catfish (*Ictalurus*

41   *punctatus*) have shown that more than 90% of suction power in high performance strikes comes

42   from the axial musculature. Thus, the shape of the axial muscles and skeleton may impact

43   suction feeding mechanics. Royal knifefish (*Chitala blanci*) have an unusual postcranial

44   morphology, with a ventrally flexed vertebral column and relatively large mass of epaxial

45   muscle. Based on their body shape, we hypothesized that royal knifefish would generate high

46   power strikes by utilizing large neurocranial elevation, vertebral column extension, and epaxial

47   shortening. As predicted, *C. blanci* generated high suction expansion power compared to the

48   other three species studied to date (up to 160 W), which was achieved by increasing both the rate

49   of volume change and the intraoral subambient pressure. The large epaxial muscle (25% of body

50   mass) shortened at high velocities to produce large neurocranial elevation and vertebral

51   extension (up to 41 deg, combined), as well as high muscle mass-specific power (up to 800 W

52   kg^{-1}). For the highest power strikes, axial muscles generated 95% of the power, and 64% of the

53   axial muscle mass consisted of the epaxial muscles. The epaxial-dominated suction expansion of

54   royal knifefish supports our hypothesis that postcranial morphology may be a strong predictor of

55   suction feeding biomechanics.

56

INTRODUCTION

High performance suction feeding in ray-finned fishes is both fast and forceful, requiring high power to expand the buccal cavity and suck in prey. Instantaneous suction expansion power can be measured empirically by using X-ray Reconstruction of Moving Morphology (XROMM) to measure instantaneous buccal cavity volume and rate of buccal cavity expansion (Camp et al., 2015). Combined with measurements of subambient buccal pressure, buccal volume measurements make it possible to calculate instantaneous suction expansion power as the product of rate of buccal volume change and subambient buccal pressure (Van Wassenbergh et al., 2015).

To date, suction expansion power has been measured with XROMM in three species of ray-finned fishes: largemouth bass (*Micropterus salmoides*), bluegill sunfish (*Lepomis macrochirus*), and channel catfish (*Ictalurus punctatus*) (Camp et al., 2015; Camp et al., 2018; Camp et al. 2020). In the highest performance strikes from all three species, the empirically measured suction power was far too great to have been generated by muscles in the head region alone. Instead, more than 90% of suction power came from epaxial and hypaxial musculature (largemouth bass and bluegill sunfish) or the hypaxial musculature (channel catfish). Furthermore, the axial musculature was found to actively shorten along 60-70% of the length of the body, encompassing the majority of axial muscle mass (Camp et al., 2015; Camp et al., 2018; Camp et al., 2020; Jimenez and Brainerd, 2020; Jimenez and Brainerd, 2021). Thus, although it has long been known that axial musculature contributes to suction feeding (Liem, 1967; Osse, 1969), the ability to measure suction power, muscle length, and activation has revealed that some fish use nearly their whole bodies for suction feeding. The overall body shape and musculoskeletal morphology should therefore be considered when studying the biomechanics and energetics of suction feeding (Camp and Brainerd, 2022).

There are several ways the morphology of the body and axial muscles, including skeletal elements linking the head and body, can impact intraoral pressure, buccal volume, and ultimately suction power. First, the shape of the body reflects the relative size and distribution of the axial muscles, which may impact their function during feeding. Carroll et al. (2004) found that deeper-bodied fish had greater epaxial cross-sectional area and longer epaxial moment arms for cranial elevation. As a result, deep-bodied bluegill sunfish were capable of greater pressure generation during feeding than the more fusiform largemouth bass (Carroll et al., 2004). Both the dorsoventral depth (Fig. 1C) and transverse shape (Fig. 1D) of the body reflect the relative cross-

89   sectional area of the epaxial and hypaxial muscles. While hypaxial muscles typically have

90   smaller cross-sectional areas anteriorly where they surround the body cavity, these muscles

91   contribute substantially to suction power in all species studied so far with XROMM.

92   Second, body shape and skeletal anatomy may influence neurocranial elevation, a

93   common component of mouth expansion and an essential motion for transmitting epaxial muscle

94   power to the head. Deep-bodied fish with more bony processes (i.e. supraneurals, neural spines,

95   and pterygiophores) immediately caudal to the neurocranium—like bluegill sunfish—had less

96   neurocranial elevation than largemouth bass (Jimenez et al., 2018; Camp and Brainerd, 2014;

97   Camp et al., 2018; Table 2). The channel catfish, which has even more postcranial ossifications,

98   uses little or no neurocranial elevation (Camp et al., 2020). Rather, catfish relied on hypaxial

99   muscle power, transmitted via retraction of their robust pectoral girdle (Camp et al., 2020). These

100   inter-species comparisons demonstrate emerging links between postcranial morphology and

101   suction feeding power and biomechanics. However, so far only a small sample of body shapes

102   and species have been investigated.

103   The royal knifefish (*Chitala blanci*) offers an interesting model for studying suction

104   feeding, as it is both morphologically and phylogenetically distinct from species previously

105   studied with XROMM. The royal knifefish is a member of the family Notopteridae (Order

106   Osteoglossiformes) and is not closely related to channel catfish (Order Siluriformes) nor

107   largemouth bass and bluegill sunfish (Order Centrarchiformes). Morphologically, royal knifefish

108   have a ventrally flexed vertebral column and depressed neurocranium in their resting posture,

109   dorsoventrally deep epaxial musculature, and laterally compressed body (Fig. 1; Coombs and

110   Popper, 1982; Sanford and Lauder, 1989). In addition, royal knifefish have an inverted teardrop

111   shaped transverse cross-section, with the body being thickest at the epaxial muscles and tapering

112   in thickness ventrally towards the hypaxials and anal fin (Fig. 1B).

113   Of the species previously studied with XROMM, bluegill sunfish have the most similar

114   body shape to royal knifefish. Both species have laterally compressed and deep bodies, ventrally

115   curved vertebral columns, and dorsoventrally deep epaxial muscles (Fig. 1). Similar to bluegill

116   sunfish, the epaxial muscles of royal knifefish provide a relatively large cross-sectional area and

117   large moment arm, which may enable them to generate similarly large subambient buccal

118   pressures. Compared to largemouth bass and channel catfish, bluegill sunfish generated the most

119   powerful suction expansion relative to their body and muscle mass, by generating greater

120   subambient buccal pressures with smaller axial muscles (Camp et al., 2018). Since royal

121 knifefish have similar epaxial morphology, we expect they can also generate powerful suction

122 expansion, relative to their muscle mass.

123 Royal knifefish also differ from bluegill sunfish in key ways, which we hypothesize will

124 result in greater neurocranial elevation and epaxial contribution in royal knifefish. Royal

125 knifefish have a more laterally compressed and craniocaudally elongated head and body, a more

126 ventrally flexed vertebral column, fewer bony processes caudal to the neurocranium, and a

127 greater proportion of epaxial muscle than bluegill sunfish. The exaggerated ventral flexion of the

128 vertebral column causes the neurocranium to have a depressed resting posture, which we expect

129 increases its range of dorsoventral motion (Fig. 1). Additionally, the curvature may cause the

130 axis of rotation of the neurocranium to be located more caudally (close to the vertebral column

131 inflection point), which has also been correlated with greater neurocranial elevation (Jimenez et

132 al., 2018). Compared to bluegill sunfish, royal knifefish have few bones immediately caudal to

133 the neurocranium: no supraneurals or dorsal fin pterygiophores, and thin neural spines. We

134 predict that this enables them to perform larger neurocranial elevation than bluegill sunfish.

135 Lastly, while both royal knifefish and bluegill sunfish have dorsoventrally deep epaxial muscles,

136 the transverse cross-section of the royal knifefish (forming an inverted teardrop) increases the

137 epaxial muscle mass relative to the hypaxials (Fig. 1). Based on the body shape of the royal

138 knifefish, we hypothesize that they rely predominantly on massive epaxial muscles and large

139 neurocranial elevation to power suction feeding.

140 To test these hypotheses, we used XROMM to measure the 3D skeletal kinematics and

141 instantaneous buccal volume of royal knifefish during suction feeding. Intraoral pressure was

142 also measured simultaneously and combined with the rate of buccal volume change to calculate

143 the suction power during royal knifefish strikes (Camp et al., 2015; Camp et al., 2020). Length

144 changes were measured throughout the epaxial, hypaxial, and sternohyoid muscles during

145 suction feeding using fluoromicrometry (Camp et al., 2016). Muscle shortening and post-mortem

146 muscle mass were used to determine the roles and relative contributions of these muscles to

147 suction power. These data allowed us to test if royal knifefish 1) have relatively large cranial

148 elevation compared to previously studied species (bass, sunfish, and catfish) and 2)

149 predominantly utilize epaxial muscle power when suction feeding. Determining how royal

150 knifefish use their unusual postcranial morphology to power suction expansion provides a better

151 understanding of the relationship between body shape and suction feeding biomechanics.

152

MATERIALS AND METHODS

Royal knifefish (*Chitala blanci*, d'Aubenton 1965) were acquired from Ocean State Aquatics, Coventry RI: Cb01 (standard length 35.6 cm, body mass 217 g), Cb03 (30.8 cm, 170 g), and Cb04 (43.3 cm, 480 g). Royal knifefish were maintained on a diet of goldfish (*Carassius auratus*). All experimental procedures were approved by Brown University Institutional Animal Care and Use Committee.

The fish were anesthetized with a buffered MS-222 solution during surgical implantation of a buccal cannula for pressure measurement and radio-opaque bone and muscle markers. Implantation techniques were consistent with those previously reported (Camp and Brainerd, 2014), and are described here in brief. One to five radio-opaque markers (tantalum spheres 0.50 or 0.80 mm in diameter) were implanted into the neurocranium, the left and right ceratohyals and cleithra, and the left maxilla, lower jaw, suspensorium, and operculum (Fig. 2A,B). Cb04 received bilateral lower jaw implantations. In all individuals, 0.80 mm tantalum beads were implanted superficially, slightly to the left of the mid-sagittal plane in the epaxial (five to nine markers), and sternohyoid musculature (two to three markers) (Fig. S1). Ventral muscles were marked in Cb01 (anal fin) and Cb04 (hypaxial) with three to five markers, with no ventral markers in Cb03. The dorsal column of epaxial musculature was implanted in Cb04 (three markers) (Fig. S1). Five to six muscle markers were used to define a body plane (Fig. S1). Following established methods, a cannula guide for the pressure transducer was implanted into the ethmo-frontal region of the neurocranium, avoiding the palatine and teeth, protruding just into the buccal cavity (Norton and Brainerd, 1993). All individuals received perioperative analgesic (butorphanol or ketoprofen) and Cb01 and Cb03 received an antibiotic (enrofloxacin). Fish were allowed to recover fully, i.e., resumed natural and aggressive feeding behaviors, before filming experiments began.

Data recording

All fish were trained to feed on live goldfish (approximately 3-5 cm total length) in custom-built acrylic aquaria with a feeding extension tunnel (75–100 mm wide, 300-400 mm long) designed to minimize the amount of water through which the X-ray beams must travel (Gidmark et al., 2012). See Movie S1 for a standard light video (recorded at 500 frames s^{-1} and slowed down 16.7 times) of Cb04 feeding in a tunnel.

184   A custom biplanar X-ray system (Imaging Systems and Services, Painesville, OH, USA)

185 was used to capture dorsoventral and lateral X-ray videos at 500 frames s^{-1} with Phantom v10

186 high-speed cameras (Vision Research, Wayne, NJ, USA) at 100 mA and 90-115 kV. Standard

187 grid and calibration objects were used to remove distortion introduced by X-ray machines and to

188 calibrate three-dimensional (3D) space (Brainerd et al. 2010). Intraoral pressure was

189 simultaneously recorded with an SPR- 407 Mikro-tip pressure probe (Millar Instruments,

190 Houston, TX, USA) inserted into the neurocranial cannula, recording at 1000 Hz with PowerLab

191 and LabChart 7.2.2 (ADInstruments, Colorado Springs, CO, USA). Pressure transducer

192 calibration was carried out daily by moving the probe through a 10 cm change in water depth

193 while recording the voltage output. This model of probe provides linear pressure-voltage outputs

194 over a pressure range of at least 0 to -60 kPa (Higham et al., 2006). Pressure data were collected

195 for each strike and noise was filtered in R (2019, R Core Team, Vienna, Austria) using a low-

196 pass, forward-backward (to remove phase shifts) Butterworth filter at a cutoff frequency of 200

197 Hz. The pressure recording was initiated by the X-ray camera trigger and corrected for a mean

198 measured lag of two milliseconds (range 1-3 ms) from the initial X-ray image. For three Cb03

199 strikes, the initial X-ray images were missing, so to correctly align the pressure and video data,

200 we averaged the time between peak pressure and peak rate of volume change for all Cb04 strikes

201 and corrected the Cb03 image sequences to account for a pressure lag of two milliseconds.

202 Feeding trials with the greatest subambient buccal pressure from each individual were chosen for

203 analysis. A total of 23 recorded strikes (six from Cb01, seven from Cb03, ten from Cb04) were

204 analyzed.

205   Computed tomography (CT) scans were taken of each fish after surgical implantation

206 with a FIDEX CT Scanner (Animage, Pleasanton, CA, USA), with 480×480 pixel resolution

207 and 0.173 mm slice thickness. From these scans, polygonal meshes of each bone and the radio-

208 opaque markers were generated in Horos (v3.3.5; Horos Project; horosproject.org) and edited in

209 Geomagic 2014 (Research Triangle Park, NC, USA). Markers were imported into Autodesk

210 Maya 2020 (San Rafael, CA, USA) and with custom scripts from 'XROMM Maya Tools'

211 package--available at https://bitbucket.org/xromm/xromm_mayatools--their respective *xyz* (3D)

212 coordinates were determined. Raw data for this study are publicly available and stored on the

213 XMAPortal (http://xmaportal.org) in the study "Knifefish Suction Feeding," with the permanent

214 identifier BROWN65. Video data are stored with their essential metadata in accordance with

215 best practices for video data management in organismal biology (Brainerd et al., 2017).

216

XROMM animation

218   For each of the three individual *C. blanci*, skeletal kinematics were reconstructed using

219   marker-based XROMM with XMALab 1.5.5 (Knörlein et al., 2016; software and instructions

220   available at https://bitbucket.org/xromm/xmalab) and custom XROMM MayaTools scripts.

221   Markers from both X-ray videos were tracked in XMALab with a mean precision of 0.05 mm

222   and maximum precision error of 0.1 mm across all trials (measured as the standard deviation of

223   the unfiltered pairwise marker-to-marker distances within all rigid bodies). Marker coordinates

224   were used to reconstruct the 3D motion of each bone using the 'matools' R package, following

225   the XROMM workflow described in Olsen et al., 2019 (available under matools R package at

226   https://github.com/aaronolsen). Briefly, all *xyz* marker coordinates were smoothed and, for bones

227   containing three or more markers, 3D coordinates were combined with their respective CT

228   coordinates (using the 'unifyMotion' function from 'matools') to produce rigid body

229   transformations. These transformations were applied to the skeletal bone meshes in Maya (2020,

230   Autodesk), producing a 3D XROMM animation of each suction feeding strike (Fig. 2A,B). For

231   any bones with only two beads or those with a linear set of markers, virtual constraints were

232   applied using the 'matools' R package in accordance with anatomical constraints (e.g.

233   cartilaginous symphysis between the cranioventral region of the left and right cleithra, or

234   ceratohyal retraction along the neurocranial mid-sagittal plane).

235   The body plane was animated with a set of five to six intramuscular axial markers in

236   roughly the same location along the body for each individual. These markers were positioned

237   near the most curved region of the vertebral column (Fig. S1). Their 3D coordinates were

238   combined with their respective CT coordinates to generate a rigid body transformation using the

239   'matools' R package (Olsen et al., 2019). The body plane animation was included in the

240   XROMM animations mentioned above.

241

Skeletal kinematics

243   Six-degree-of-freedom motions of the neurocranium and left cleithrum were measured

244   relative to the body plane. These rotations were measured with a joint coordinate system (JCS),

245   which measures the relative rotations of two anatomical coordinate systems (ACSs), one

246   attached to the bone and the other to the body plane (Camp and Brainerd, 2014; Camp et al.,

247   2018). Each JCS measured translation and Euler angle rotations about the x-, y-, z- axis,

248   following the right-hand rule and *zyx* order of rotation. The JCS used to measure neurocranial

249   motion was placed at the craniovertebral joint and the JCS to measure cleithral motion was

250   placed at the dorsal tip of the cleithra. Both sets of JCSs were aligned with the z-axis oriented

251   mediolaterally, y-axis rostrocaudally, and the x-axis dorsoventrally. Z-axis rotations were

252   standardized to start at 0 deg by subtracting their value at the start of each strike. Positive

253   rotation about the z-axis reflects dorsal rotation in the sagittal plane, corresponding to

254   neurocranial elevation or cleithral protraction. Rotations about the z-axis also reflect dorsoventral

255   motions of the cranial vertebrae, as these impact the position and motion of the body plane.

256

257   **Dynamic endocast**

258   Following previously established methods, changes in buccal cavity volume were

259   measured from XROMM animations using a dynamic endocast (Camp et al., 2015; Camp et al.,

260   2020). In brief, a polygonal mesh endocast of the left side of the buccal cavity was generated

261   using locators attached to the inside surface of cranial bones. Additional locators were placed

262   between bones to define the ventral border of the buccal cavity, i.e., the sternohyoid and

263   protractor hyoideus muscles, and the mid-sagittal plane dividing the left and right sides of the

264   buccal cavity. The 3D coordinates of the locators were imported into MATLAB (R2020a;

265   MathWorks, Natick, MA, USA) and custom-written scripts (available at

266   https://bitbucket.org/ArielCamp/dynamicendocast) were used to generate the volume enclosing

267   the locators and calculate its volume, for each frame. For each frame, the volume was generated

268   from the xyz coordinates of the locators using an alpha shape: a method of fitting or "wrapping"

269   3D points with a 3D shape (Edelsbrunner et al., 1983). Alpha shapes are a generalization of

270   convex hulls that allow the fineness of fit to be varied by changing the alpha value and allows the

271   shape to include concave curvatures. The volumes were generated using the 'alphashape'

272   function in MATLAB, and an alpha value of 3 was found to provide the best fit, i.e., endocasts

273   fully filled the mouth cavity with minimal interpenetration of the bone models. Polygonal

274   meshes (.obj files) of the volumes of the left side of the buccal cavity were then imported into

275   Maya for visual verification (Fig. 2E,F). Under assumptions of bilateral cranial symmetry, the

276   left mesh volume was doubled to calculate bilateral buccal volume expansion.

277

278   **Muscle length changes**

279   Sternohyoid and axial muscle length changes were measured from X-ray videos as the

280   distance between intramuscular markers, i.e., by fluoromicrometry (Camp et al., 2016). Muscle

281   markers were tracked in XMALab and their coordinates were filtered in R with 'matools' as

282   described above. The distance between muscle markers was subsequently calculated in R to

283   determine the magnitude and distribution of sternohyoid, epaxial, and hypaxial muscle

284   shortening. To capture muscle shortening in the cranialmost region of the epaxial muscle and the

285   dorsal column of Cb04, the distance was measured between the first marker in the muscle region

286   and a locator placed at the cranialmost neurocranium-epaxial muscle attachment site of the

287   animated neurocranium model in Maya. Distance in the cranialmost hypaxial region was

288   calculated between the first hypaxial muscle marker and a locator attached to the cleithra, placed

289   in line with the hypaxial muscle bead set (Fig. S1). Since the entire marker set was not

290   consistently within the X-ray imaging volume, axial muscle length was measured from a subset

291   of axial muscle markers that were visible in almost all strikes. This set of markers extended

292   approximately 7-9 cm caudal of the craniovertebral joint: from the neurocranium to as far back

293   as a few centimeters cranial of the dorsal fin (Fig. S1). Within this region, fluoromicrometry was

294   used to estimate the muscle lengths of subregions along the length of the body by measuring

295   distance between adjacent pairs of intramuscular markers.

296   For the axial muscles, whole-muscle length was calculated by taking the sum of the

297   subregional muscle lengths, originating with the cranialmost locator and extending to the

298   caudalmost visible muscle marker. In the sternohyoid, all implanted markers were visible, and its

299   measurements are reported as whole-muscle length. Muscle length at each time step was

300   normalized by the mean initial length measured at the first recorded frame of each strike (L_i),

301   with values less than one representing that the muscle had shortened. Muscle velocity was

302   similarly calculated at each time as the change in normalized muscle length divided by the

303   change in time, denoted by L_i s^{-1}, with positive values representing muscle shortening. Note that

304   this method for determining axial muscle strain differs slightly from other suction power studies,

305   in that we used the sum of the subregional muscle lengths, whereas prior papers used the

306   distance from the neurocranium or cleithrum to the caudalmost axial muscle marker (Camp et al.,

307   2015; Camp et al., 2018; Camp et al., 2020). The summation method recorded more consistent

308   levels of epaxial muscle shortening in *C. blanci*, likely due to its ability to capture the length of

309   the naturally flexed epaxial musculature at rest.

310

Power calculations

311

312 Instantaneous suction power was calculated in R as the product of rate of volume change

313 and intraoral pressure as described in Camp et al. (2015). Before calculating rate of volume

314 change, bilateral buccal volume measurements from the dynamic endocast were filtered with a

315 low-pass, forward-backward Butterworth filter (150 Hz cutoff) to reduce noise generated by

316 frame-to-frame polygonal mesh re-triangulations. Buccal pressure was downsampled from 1000

317 Hz to 500 Hz to match the frequency of the volume data. Pressure data were calculated relative

318 to initial, ambient pressure prior to the strike and multiplied by -1, so that at each time step, the

319 product of subambient pressure and increasing rates of volume change would reflect positive

320 power (Fig. 3).

321 For each strike, axial and cranial mass-specific power were calculated by dividing the

322 maximum instantaneous power by the mass of the respective muscle groups. Muscle masses

323 were determined by post-mortem dissection of the muscle regions on the right side of the fish,

324 weighed on a digital scale, and then doubled to estimate bilateral muscle mass for all individuals

325 except Cb03. The body of Cb03 was unavailable for dissection, so muscle masses are estimates

326 determined by averaging the percent of muscle mass for each muscle of Cb01, Cb04, and an

327 additional individual, Cb02, and assuming proportionality based on overall body mass across

328 individuals (Table 1). The total body mass, and bilateral epaxial, hypaxial, dorsal column,

329 sternohyoid, and cranial muscle masses from Cb02 were 0.393 kg, 0.103 kg, 0.066 kg, 0.002 kg,

330 0.0032 kg, and 0.0054 kg respectively (values for other individuals are reported in Table 1). In

331 accordance with previous XROMM studies, epaxial muscle mass included all of the epaxial

332 musculature dorsal to the vertebral column and about 60-70% along the length of the body, based

333 on the extent of shortening identified (Camp and Brainerd, 2014; Camp et al., 2018; Camp et al.,

334 2020; Jimenez and Brainerd, 2020; Jimenez et al., 2021). Note that this method differs from prior

335 studies, which only included epaxial musculature dorsal to the cleithrum-supracleithrum joint,

336 and which reported lower percentages of epaxial muscle mass in bluegill sunfish and largemouth

337 bass (Carroll, 2004; Carroll and Wainwright, 2009). Axial mass-specific power was calculated

338 by dividing instantaneous power by the sum of the epaxial, hypaxial, and dorsal column muscle

339 mass. Cranial mass-specific power was calculated by dividing instantaneous power by the

340 combined mass of the levator arcus palatini, dilator operculi, levator operculi, and sternohyoid

341 muscles. Muscle mass-specific power was determined by dividing the maximum instantaneous

342 power by the total mass of the muscle regions (epaxial, hypaxial, and sternohyoid muscle)

343 shortening during suction expansion (Fig. 3). These mass-specific values represent the estimated

344 amount of power each group of muscles would need to output if they were the sole contributors

345 to suction feeding expansion.

346   The dynamic endocast volume and buccal pressure measurements do introduce sources of

347 error in the suction power estimates, as described in Camp et al. (2018). In brief, absolute

348 volume measurements are overestimates, since they do not account for the presence of soft tissue

349 or internal structures. However, the volume of these structures is consistent throughout the strike

350 and should have little effect on the calculations for rate of volume change and subsequent power

351 calculations. Rapid re-triangulation of dynamic endocast polygonal meshes may cause increased

352 recorded rates of volume change, however, a low-pass, forward-backward Butterworth filter with

353 a high cutoff frequency over the endocast buccal volume trace may produce underestimates of

354 the actual rate of volume change. The intraoral pressure cannula only provides pressure readings

355 at one location within the buccal cavity and does not capture variations in pressure during

356 suction feeding (Muller et al., 1982; Van Wassenbergh, 2015). These estimates are likely

357 underestimates of subambient pressure, since modeling of clariid catfishes and bluegill sunfish

358 (Van Wassenbergh et al., 2015) and *in vivo* measurements (Tegge et al., 2020) suggested that

359 highest subambient pressure occurred more caudally in the buccal cavity (Van Wassenbergh et

360 al., 2005; Van Wassenbergh et al., 2006b). Additionally, our power calculations do not account

361 for the forces required to overcome inertia or drag (Van Wassenbergh et al., 2015), yet studies of

362 clariid catfishes and largemouth bass indicate that these forces are likely small compared to that

363 required to overcome subambient pressure (Van Wassenbergh et al., 2005; Van Wassenbergh et

364 al., 2015). Therefore, our values for instantaneous suction power are most likely to be

365 underestimates.

366

367 **Determining peak gape**

368   Suction feeding power, muscle shortening, and skeletal kinematics were all measured

369 relative to the time of peak gape. Gape distance was measured as the distance between virtual

370 locators on the rostralmost tips of the lower jaw and premaxilla. Peak gape is defined here as the

371 maximum gape distance directly following the rapid increase in gape during the start of the

372 strike. We calculated this by identifying the first frame at which there is a major change in the

373 inflection of the gape distance curve from increasing to decreasing or in some cases minimal

374 increasing. By taking the derivative of gape distance over time, we used 10% of the maximum

375   rate of gape change as a threshold to isolate the first time point when the rate of gape change was

376   below the threshold (Fig. S2). This method for determining peak gape differs from other suction

377   power studies (Camp et al., 2015; Camp et al., 2018; Camp et al., 2020), but was chosen because

378   of the high variability of gape distance traces in royal knifefish, e.g., gape curves with multiple

379   peaks (double-strikes) or initial strikes followed by slow gradual gape expansion (slowly

380   increasing plateau). Selecting the initial peak gape frame using the first instance of major

381   inflection in gape distance yielded substantially better consistency of alignment of the expansion

382   part of the gape cycle in this study (Fig. S2).

383

384   **RESULTS**

385   In our study, royal knifefish were capable of generating very high suction power (Fig. 4).

386   The neurocranium reached high magnitudes of elevation during the period of peak power (Fig.

387   5). Similarly, the epaxial muscle generated high strain and shortening velocity, reaching its

388   shortest length during the period of peak power, and the sternohyoid shortened consistently

389   across all strikes (Fig. 5). In addition, muscle mass-specific power was unusually high in the

390   highest power strikes, reaching 535 W kg^{-1} in Cb03 and 800 W kg^{-1} in Cb04 (Fig. 4).

391

392   **Inter-individual variation**

393   Cb04 produced substantially higher power strikes than Cb01 and Cb03 (Fig. 4). The

394   mean peak power for Cb04 was 15 times greater than Cb01 and 6 times greater than Cb03 with

395   the most powerful strikes reaching 13.5 W for Cb01, 38.0 W for Cb03, and 163.3 W for Cb04.

396   The substantially larger suction power in Cb04 resulted from both greater subambient buccal

397   pressure and faster rate of buccal volume change (Table 1). In Cb04, mean peak subambient

398   pressure was approximately 5.6 times greater than that of Cb01 and nearly 3 times greater than

399   that of Cb03, and mean peak rate of volume change was approximately 3 times greater than

400   Cb01 and Cb03 (Table 1). Unlike Cb04, the difference in suction power between Cb01 and Cb03

401   was largely due to the difference in mean peak subambient buccal pressure, which was nearly

402   two times larger in Cb03 compared to Cb01 (Table 1). Because of these differences among

403   individuals, results are reported separately for each individual, with means and s.e.m. (Table 1).

404

405   **Skeletal kinematics**

406   The neurocranium consistently elevated (rotated dorsally) relative to the body plane,
407   across all strikes in all individuals (Fig. 5). During suction expansion, as the vertebral column
408   extended from curved to straight, the cranialmost vertebrae elevated with the neurocranium (Fig.
409   2A,B). Due to placement of our body plane, the neurocranium JCS captures a combination of
410   neurocranium elevation at the craniovertebral joint and vertebral column extension. While the
411   magnitude of rotation was sensitive to location of the body plane, the neurocranium and anterior
412   vertebral column elevated notably and consistently in all three individuals regardless of the body
413   plane's location. The mean maximum elevation measured during the period of peak power was
414   17.0 ± 3.6 deg for Cb01, 26.9 ± 4.9 deg for Cb03, and 27.9 ± 1.7 deg for Cb04. For some strikes,
415   the neurocranium showed a pattern of initial elevation, slight depression, and then continued
416   elevation at the end of pectoral girdle retraction. The initial phase of neurocranial elevation
417   occurred during the period of peak power (shown in red in Fig. 5) and during epaxial muscle
418   shortening (Fig. 5).
419   Cleithral retraction (caudoventral rotation) relative to the body plane was consistent
420   within Cb04 strikes, but highly variable in Cb01 and Cb03 (Fig. 5). During Cb04 strikes, the
421   cleithrum initially protracted (craniodorsal rotation), followed by the start of retraction prior to
422   the period of peak power, and a steady, continued retraction through the period of peak power
423   (Fig. 5). It should be noted that cleithral protraction occurs relative to the body plane; the cleithra
424   are not protracting relative to the neurocranium but are instead being pulled dorsally by vertebral
425   column extension, causing hypaxial lengthening. Maximum cleithrum retraction in Cb04
426   averaged -3.1 ± 0.6 deg during the period of peak power and increased to an average of $-6.4 \pm$
427   0.5 deg after the period of peak power. Cb01 and Cb03 showed variability in timing and did not
428   always retract during the period of peak power in their strikes. The magnitude of cleithral
429   protraction and retraction was also highly variable in Cb01 and Cb03 (Fig. 5), with mean peak
430   retractions of -3.0 ± 2.7 deg and 0.8 ± 3.0 deg, respectively, during the period of peak power.
431
432   **Muscle length changes and muscle power**
433   The epaxial and sternohyoid muscles consistently shortened prior to and during peak
434   power in all individuals (Fig. 5). However, the magnitude and pattern of epaxial shortening
435   varied across individuals. Epaxial muscles shortened across all of the measured subregions in
436   Cb03 and Cb04, and all but the caudalmost subregion of Cb01 (Fig. 6). Mean peak whole-muscle
437   strain in the epaxials during the period of peak power was similar between Cb04 and Cb03 ($8.0 \pm$

438   0.7 % L_i and 7.9 ± 1.4% L_i, respectively), as was mean peak muscle shortening velocity during

439   the period of peak power (4.7 ± 0.1 L_i s^{-1} and 4.6 ± 1.5 L_i s^{-1}, respectively). Epaxial strains

440   during the period of peak power were lower in Cb01, less than half that of Cb03 and Cb04

441   (Table 1). Mean peak epaxial strain during the period of peak power was lowest in the

442   cranialmost region (below 5% strain in all individuals) and the highest at approximately one-half

443   to three-fourths of the distance between the craniovertebral joint to the dorsal fin (3-6 cm, 4-7

444   cm, and 6-8 cm caudal of the craniovertebral joint in Cb01, Cb03, and Cb04, respectively) (Fig.

445   6; Fig. S1).

446   Similar shortening behaviors were seen in the dorsal column of muscle of Cb04, the only

447   individual with beads implanted in this muscle (Fig. S3). This column of muscle is dorsal to and

448   separate from the epaxial. It inserts on the neurocranium and extends along the length of the

449   body. The dorsal column of Cb04 shortened at the same time as the corresponding region of the

450   epaxial muscle (three cranialmost subregions), reaching 5.8 ± 0.4 % L_i strain and muscle

451   shortening velocity of 3.4 ± 0.1% L_i s^{-1} (Fig. S3). The caudalmost subregion showed the greatest

452   magnitude of strain.

453   In the hypaxial musculature of Cb04, a consistent pattern of lengthening then shortening

454   prior to the period of peak power occurred in all recorded strikes (Fig. 5). Early lengthening

455   across the full extent of the marked hypaxial muscle was so great in Cb04 that, during peak

456   power, it shortened with a mean peak velocity of 4.1 ± 0.1 L_i s^{-1}, while the muscle length was

457   still longer relative to its initial length (-1.1 ± 0.4% L_i) (Table 1). The caudalmost subregion of

458   the hypaxial muscle shortened during the period of peak power, while the cranialmost subregions

459   lengthened (Fig. 6). Unlike Cb04, ventral muscle beads in Cb01 were implanted in the anal fin

460   musculature, and no beads were implanted in the hypaxial muscle of Cb01 or Cb03 (Fig. S1).

461   The shortening patterns and strain of the ventral muscle beads in Cb01, during the period of peak

462   power, were highly variable (1.8 ± 2.8% L_i) (Fig. 5, Table 1).

463   The sternohyoid shortened with a consistent pattern in all strikes and across individuals,

464   with mean strains of 2.5-2.7% during the period of peak power (Table 1, Fig. 5). Sternohyoid

465   shortening began prior to and continued through the period of peak power, with higher

466   shortening velocities occurring during peak power. Magnitudes of strain in the sternohyoid were

467   similar across individuals, but sternohyoid shortening velocity during the period of peak power

468   was up to two times higher in Cb04 and Cb03 compared to Cb01 (Table 1).

469   Royal knifefish generated high muscle mass-specific power, which we calculated by

470   dividing the maximum instantaneous suction power of each strike by the total mass of

471   musculature shortening during peak power generation (epaxial, hypaxial and sternohyoid). For

472   these muscles (0.2035 kg combined for Cb04) to produce the highest power strike recorded

473   (163.3 W), they would have needed to generate 802.5 W kg^{-1} of power. The next three highest

474   power strikes recorded for Cb04 are estimated to have required 628.0 W kg^{-1}, 565.0 W kg^{-1}, and

475   545.0 W kg^{-1}. The maximum peak muscle power in Cb01 was much lower (164.2 W kg^{-1}), but

476   the muscle power in the highest power strike in Cb03 (535.3 W kg^{-1}) was within the range of

477   muscle power generated across all Cb04 trials (289.3 W kg^{-1} - 802.5 W kg^{-1}).

478

479   **DISCUSSION**

480   The massive epaxial muscles of royal knifefish account for >25% of body mass and

481   during suction feeding they shortened considerably and rapidly, generating large neurocranial

482   elevation and vertebral extension. These results agree with our predictions based on body shape

483   and postcranial morphology. During the most powerful strikes, the hypaxials also shortened and,

484   together with the epaxials, generated over 95% of the power for suction expansion with muscle

485   power output of up to 800 W kg^{-1}. The magnitude of sternohyoid muscle shortening was

486   consistent across all strikes, while the magnitude of axial muscle shortening was more variable

487   during lower power strikes. This suggests that the sternohyoid muscle may contribute a greater

488   proportion of power in lower power strikes. Likely driven by their large neurocranial elevation

489   and rapid epaxial shortening, royal knifefish generated much higher rates of buccal expansion,

490   subambient intraoral pressure, and suction power than those previously measured in other

491   species (Table 2). For the purpose of this discussion, we will compare the highest performing

492   individuals, using them as a proxy for the relative capabilities of each species (see *Variation in*

493   *suction power* section).

494

495   **Epaxial muscle shortening and neurocranial elevation**

496   During suction feeding, royal knifefish substantially elevated their neurocranium and

497   cranialmost vertebrae, fully straightening their vertebral column (Fig. 2). Mean maximum

498   neurocranial elevation during the period of peak power in royal knifefish exceeded the mean

499   maximum neurocranial elevation values previously measured in largemouth bass, bluegill

500   sunfish, and channel catfish (Table 2). The highest values of neurocranial elevation during the

501   period of peak power recorded in each royal knifefish individual (28-42 deg) were within the

502   range observed in Commerson's frogfish (*Antennarius commerson*), a genus known for its

503   exceptionally large suction expansion (Camp, 2021; Longo et al., 2016). Our results are

504   consistent with the predictions that a combination of the initially depressed neurocranium and

505   ventrally flexed vertebral column increased the range of neurocranial motion used during suction

506   feeding. Interestingly, these are anatomical traits shared by the frogfish (Camp, 2021) but not all

507   species with extremely high cranial elevation (Lauder and Liem, 1981; Van Wassenbergh et al.,

508   2008).

509   In royal knifefish, the epaxial musculature shortened along at least 60-70% of the body

510   length, with high strain and shortening velocity. When comparing the highest performing

511   individual of each species, the mean peak epaxial muscle strain during the period of peak power

512   of royal knifefish was approximately two times the absolute peak epaxial strain (which occurred

513   after the period of peak power) of largemouth bass and bluegill sunfish (Table 2). Similarly, the

514   mean peak epaxial shortening velocity during the period of peak power was more than two times

515   higher in the highest performing individual in royal knifefish than in largemouth bass and

516   bluegill sunfish (Table 2). While the maximum shortening velocity (V_{max}) for royal knifefish

517   epaxials is unknown, V_{max} for largemouth bass has been measured as 11 L_i s^{-1} (Coughlin and

518   Carroll, 2006), with 3-4 L_i s^{-1} as the range expected for optimal power output. Epaxial shortening

519   velocity during the period of peak power in the highest performing royal knifefish was 4-5 L_i s^{-1},

520   suggesting that the epaxials may be shortening at or near the range for optimal power output.

521

Hypaxial muscle shortening and cleithral retraction

523   In Cb04, the cleithrum consistently protracted then retracted, while the hypaxial muscles

524   lengthened then shortened. Cleithral protraction and hypaxial lengthening corresponded to the

525   start of neurocranial elevation and vertebral column extension, which likely pulled rostro-

526   dorsally on the cleithrum relative to the body plane, substantially lengthening the hypaxials. This

527   pattern of cleithral protraction and hypaxial lengthening prior to cleithral retraction and hypaxial

528   shortening has not been observed in ray-finned fishes previously studied with XROMM.

529   Although this rostro-dorsal motion was measured as cleithral protraction, the cleithrum did not

530   appear to protract relative to the neurocranium and we did not observe a reduction in buccal

531   volume. Because the vertebral column remained partially extended after peak extension,

532   shortening of the hypaxials back to just their initial length still retracted the cleithrum, on

533   average, -6.4 ± 0.2 deg past its initial position (Fig. 5). Compared to the highest performing

534   individual of each species, royal knifefish had greater mean peak hypaxial shortening velocity

535   during the period of peak power than bluegill sunfish and more than 2.5 times that of largemouth

536   bass and channel catfish (Table 2).

537   While the ventral muscle markers in Cb01 were implanted ventral to the hypaxial muscle,

538   in the anal fin muscle (Fig. S1), the muscle length traces seemed to align with the cleithral

539   retraction patterns as in Cb04 (Fig. 5). This suggests that anal fin data may still be reflective of

540   hypaxial strain, but possibly more variable in lower power strikes.

541

542   **Relative contributions of the epaxial and hypaxial muscles**

543   Our results suggest that the epaxial muscles are generating a greater portion of suction

544   power than the hypaxial muscles in royal knifefish. First, mean epaxial muscle mass was 1.8

545   times greater than the hypaxial muscle mass, and so was capable of greater power output (Table

546   1). Second, in Cb01 and Cb03, cleithrum retraction—and presumably hypaxial shortening—were

547   inconsistent, while neurocranial elevation and epaxial shortening were large and consistent (Fig.

548   5; Table 1). Although Cb04 used consistent cleithral retraction and hypaxial shortening, the

549   magnitude and speed of hypaxial strain was less than half of epaxial strain (Table 1, Table 2).

550   These data support the conclusion that the hypaxial muscles contributed less power, less

551   consistently to suction expansion than the epaxial muscles.

552

553   **Sternohyoid muscle shortening and contributions to suction power**

554   The timing and magnitude of sternohyoid shortening were relatively consistent across all

555   strikes, irrespective of suction power and individual. All individuals had similar mean

556   magnitudes of peak strain during the period of peak power, within 2.5-2.7 % L_i (Table 1). The

557   sternohyoid shortened during the period of peak power and is electrically active during feeding

558   strikes in congeneric species (Sanford and Lauder, 1989), which suggests that it actively

559   contributed power to buccal cavity expansion. Consistent sternohyoid shortening similarly

560   occurred during buccal cavity expansion in channel catfish, bluegill sunfish, striped surfperch

561   (*Embiotoca lateralis*), and one clariid catfish (Camp et al., 2018; Camp et al., 2020; Lomax et

562   al., 2020; Van Wassenbergh et al., 2007a). By contrast, in largemouth bass and several clariid

563   catfishes, the sternohyoid did not shorten (or lengthen) during rapid suction expansion but rather

564   acted as a stiff ligament that transmitted power from hypaxial musculature to produce hyoid

565   depression (Camp and Brainerd, 2014; Van Wassenbergh et al., 2007a). Because the sternohyoid

566   did not lengthen in royal knifefish, it also transmitted power generated from hypaxial shortening

567   to facilitate hyoid depression and buccal expansion. This suggests that the sternohyoid has a dual

568   function in royal knifefish, both transmitting power from the hypaxial muscle and generating

569   power by shortening during the period of peak power.

570   The consistent pattern of sternohyoid shortening across all individuals suggests that the

571   sternohyoid muscle may provide a greater proportion of muscle power in low performance

572   strikes. To generate the suction power for the highest recorded strike in Cb04, we estimated that

573   the musculature would need to generate 802.5 W kg^{-1}. At this maximum muscle mass-specific

574   power the sternohyoid in Cb04 (0.0046 kg) would be able to generate 3.7 W, which is within the

575   range of the lowest power strikes recorded in Cb01 and Cb03. Similarly, the sternohyoid in Cb01

576   (0.002 kg) could produce up to 1.6 W of power, which is more than is necessary for suction

577   expansion in the lowest power strike (1.1 W) from Cb01. It is still unlikely that the sternohyoid

578   is the sole contributor since the neurocranium elevates and the epaxials shorten to some degree in

579   all strikes (Fig. 5). Instead, the sternohyoid may make a greater contribution to generating

580   suction power when epaxial shortening is low and hypaxial muscle shortening is inconsistent, as

581   observed in Cb01 (Fig. 5). These results suggest that high power strikes depend nearly

582   exclusively on axial muscle shortening, whereas a greater proportion of muscle power may come

583   from the sternohyoid muscle in lower power strikes.

584

585   **Variation in suction power**

586   Royal knifefish are capable of generating very high suction power, but we observed a

587   wide range of power across the three individuals. Cb04 produced substantially higher power

588   strikes, with mean peak suction power more than 15 times greater than Cb01 and 6 times greater

589   than Cb03 (Fig. 4). The higher performance of Cb04 is partially explained by its body mass

590   being more than twice the masses of Cb01 and Cb03 (Table 1), providing more muscle mass for

591   power generation. When normalizing for body mass, there was substantial overlap in the mass-

592   specific power in Cb03 and Cb04 (Fig. 7B), despite the non-overlapping ranges in absolute

593   suction power (Fig. 7A). Additionally, it is possible that larger individuals generate more power

594   per unit muscle mass if muscle power scales with positive allometry in royal knifefish as in other

595   fish species (Carroll et al., 2009; Van Wassenbergh et al., 2007b). These features account for

596   some of the variation between Cb03 and Cb04, suggesting that Cb04 may not merely be an

597   exceptional individual.

598   However, body size does not completely explain intraspecific variation in power. While

599   Cb03 had the smallest total body mass (78% of that of Cb01), it generated more than double the

600   mean peak intraoral pressure and mean peak power compared to Cb01 (Fig. 4, Table 1).

601   Interestingly, Cb01 and Cb03 had the same mean peak rate of buccal volume change. These

602   results reflect that there is not a simple relationship between buccal volume change, intraoral

603   pressure, and power, but instead a complex interaction between multiple factors, including gape

604   size (morphologically and throughout the strike), initial buccal volume, magnitude of buccal

605   volume change, timing of peak rate of buccal volume change, and timing of peak buccal cavity

606   expansion (Van Wassenbergh et al., 2005; Van Wassenbergh et al., 2006a; Van Wassenbergh et

607   al., 2006b). Motivation almost certainly contributed to this variation as well. Despite efforts to

608   standardize prey type, prey size, and training, Cb04 responded better to training, was less timid

609   when feeding in front of researchers, and was highly food motivated.

610   The variation among royal knifefish individuals is similar to what has been observed in

611   bluegill sunfish, largemouth bass, and channel catfish. In all of these species, the highest

612   performing individual generated mean body mass-specific suction power that was 2.0-2.6 times

613   higher than the second highest performing individual (Camp et al., 2015; Camp et al., 2018;

614   Camp et al., 2020). In addition, wide ranges of maximum suction power, intraoral pressure, and

615   buccal volume change were observed, even when accounting for body or buccal volume size.

616   Both the present study and previous suction power studies are unlikely to have captured

617   the maximum performance of any of these species, given the difficulty of eliciting maximum

618   performance in lab-based studies with artificial environments and small sample sizes (Astley et

619   al., 2013). Therefore, even the highest power strikes, such as those of Cb04, are conservative

620   estimates of the suction power capacity of these species. Without having captured the true

621   maxima of each species, conclusions from interspecies comparisons can only be drawn from the

622   data that has been collected. Thus, while royal knifefish suction expansion appears impressively

623   powerful compared to previously measured species, it is difficult to directly compare suction

624   power capacity across species.

625   Within these limitations, comparing the data from the four species studied to date is a

626   useful first step in exploring suction power across teleost fishes. When comparing across species,

627   it may be most appropriate to compare high performing individuals to each other and lower

628   performing individuals to each other. Within that context, all royal knifefish individuals

629   outperformed largemouth bass, channel catfish, and bluegill sunfish individuals: Cb01 and Cb03

630   outperformed the lower performing individuals, just as Cb04 outperformed the highest

631   performing individuals of those species (Fig. 7).

632

633   **Suction power, intraoral pressure, and buccal expansion**

634   Royal knifefish generated higher suction power than the other species studied to date by

635   producing both a greater magnitude of subambient intraoral pressure and a greater speed of

636   buccal expansion (Camp and Brainerd, 2022). Of the four species, the mean peak intraoral

637   pressure was greatest in royal knifefish, followed by bluegill sunfish, channel catfish, and

638   largemouth bass (Table 2). Prior studies have not found consistent effects of body size on

639   subambient buccal pressure, so we do not scale pressure here for body size (Carroll et al., 2004;

640   Carroll et al., 2009). However, it is unclear how best to compare the rate of volume change

641   among different sized individuals. If we simply compare the raw values across the highest

642   performing individual within each species, the mean peak rate of buccal volume change was

643   greatest in royal knifefish, more than 2.5 times that of largemouth bass and channel catfish, and

644   more than 6.5 times that of bluegill sunfish (Table 2). If we normalize by body mass across the

645   highest performing individual within each species, the mean peak body mass-specific rate of

646   buccal volume change was still greater in royal knifefish, more than double that of bluegill

647   sunfish and largemouth bass and almost five times that of channel catfish (Table 2). Thus, in

648   comparison to the species previously studied with XROMM, the highest performing royal

649   knifefish individual generated greater mean power by expanding its buccal cavity two times

650   faster, relative to body mass, and generating at least 1.3 times greater buccal pressure magnitude.

651   Among the highest performing individuals of each species, royal knifefish generated a

652   mean peak suction power approximately 8 times greater than channel catfish and bluegill sunfish

653   and 13 times greater than largemouth bass (Fig. 7A; Table 2). When suction power was

654   normalized by body mass or by maximum change in buccal volume—the difference between the

655   volume of maximum buccal expansion and initial volume—then royal knifefish still

656   outperformed the other three species but are more similar to bluegill sunfish (Fig. 7B,C).

657

658   **Muscle mass-specific power**

659   For high performance strikes, royal knifefish depend on the axial musculature shortening

660   at high velocities to produce large neurocranial elevation and rapid buccal expansion. At least

661   96.4% of the power for the highest power strike from Cb04 must have come from the axial

662   musculature, based on the relative masses of the head and body muscles. If the major cranial

663   muscles in Cb04 (sternohyoid, 4.6 g; levator arcus palatini, 1.64 g; levator operculi, 1.04 g;

664   dilator operculi, 0.024 g) operated at the maximum muscle mass-specific power observed (802.5

665   W kg^{-1}), the cranial muscles could generate 5.9 W of power. For Cb04, 5.9 W is just 3.6% of the

666   maximum suction power and 4.6-5.3% of the next three highest power strikes. These results are

667   consistent with the findings of previous studies, which have shown that cranial muscles are only

668   capable of contributing a small proportion of the power necessary for high performance suction

669   feeding and that the axial muscles are the primary source of suction power (reviewed in Camp

670   and Brainerd, 2022).

671   Although we expected that royal knifefish would depend on their axial muscles to

672   generate high power strikes, we did not expect the axial muscles to operate at such high muscle

673   mass-specific power in the most powerful strikes. Compared to mean muscle mass-specific

674   power outputs of the highest performing largemouth bass (74.2 ± 13.2 W kg^{-1}), bluegill sunfish

675   (267.0 ± 49.2 W kg^{-1}), and channel catfish (96.4 ± 20.1 W kg^{-1}), Cb04 achieved a greater mean

676   muscle mass-specific power output of 494.3 ± 51.6 W kg^{-1} (Table 2), with a maximum of 802.5

677   W kg^{-1}. This maximum muscle mass-specific power output is near or potentially beyond the

678   expected limits for vertebrates (Altringham et al., 1993; Askew and Marsh, 2001; Curtin et al.,

679   2005), suggesting several possible explanations: 1) we overestimated suction power; 2) we

680   underestimated the longitudinal extent of the axial musculature that is contributing suction

681   power; 3) there is power amplification, in which the muscle shortens before the skeletal elements

682   begin to move, thereby loading serial elastic elements that release their energy while the muscle

683   continues to contract as the bones move (Astley and Roberts, 2012).

684   In considering this first explanation, our suction power estimates are conservative

685   because we measured buccal pressure in one rostral location and hydrodynamic modeling has

686   shown that pressure can be even more subambient in the caudal buccal cavity (Van

687   Wassenbergh, 2015). For the second, we dissected and included the mass of nearly 75% of the

688   total epaxial and hypaxial length (Fig. S1), extending more caudally than our implanted marker

689   set in order to provide a generous muscle mass estimate. The third possibility is power

690   amplification, as is seen in the epaxial musculature of pipefishes and seahorses (Van

691   Wassenbergh et al., 2008; Van Wassenbergh et al., 2014). This is an exciting potential

692   explanation, but our results do not support this hypothesis. If power amplification were to create

693   a catapult-like mechanism, we would expect to see gradual muscle shortening prior to the

694   beginning of the strike to store elastic energy in the muscle and connective tissues (Astley and

695   Roberts, 2012; Van Wassenbergh et al., 2008). However, there was no indication of muscle

696   shortening prior to the beginning of neurocranial elevation nor pectoral girdle retraction (Fig. 5).

697   We conclude that power amplification is unlikely the cause of such high muscle mass-specific

698   muscle power estimates and that Cb04 was able to power suction feeding directly with 550-800

699   W kg^{-1} of muscle power in its four most powerful suction strikes.

700

Concluding remarks

702   Compared to the three species previously studied with XROMM, royal knifefish are

703   distinct in the morphology of their postcranial musculoskeletal system and their reliance on

704   epaxial muscles for suction feeding. In royal knifefish, their epaxial muscles were greater in

705   mass relative to the hypaxial muscles and shortened rapidly, producing a majority of suction

706   power with rapid neurocranial elevation. We expect that species with similar morphology

707   (including a ventrally flexed vertebral column, dorsoventrally deep epaxial muscles, few bones

708   immediately caudal to the neurocranium, and a high proportion of epaxial muscle mass) can also

709   produce high power strikes that are generated predominantly by epaxial muscle power and that

710   utilize large neurocranial elevation. Our results support the growing evidence that postcranial

711   morphology is important for understanding suction feeding mechanics, and that these feeding

712   functions have likely shaped the evolution of the axial muscles and skeleton. Royal knifefish

713   used nearly their entire body musculature to generate their most powerful strikes, broadening the

714   morphological and phylogenetic range of suction feeding fishes known to power feeding with

715   body muscles. However, the sternohyoid muscle likely contributed a greater proportion of power

716   in the lowest performance strikes, demonstrating that the roles of cranial and axial muscles may

717   vary not only across species, but also among feeding behaviors. Further studies examining the

718   cranial and axial musculoskeletal systems—and their interaction—are needed to understand how

719   the morphology of the whole body shapes the evolution and mechanics of suction feeding.

720

ACKNOWLEDGEMENTS

722   We are grateful to Erika Tavares for research administrative support and manuscript edits, to

723   Peter Falkingham and Stephen Gatesy for their assistance in developing the methods for the

724   dynamic digital endocast, to David Baier for the XROMM Maya Tools, and to Jake Parsons,

725   Noah Sims, and Paola Vazquez for their assistance tracking videos.

726

727   **COMPETING INTERESTS**

728   We declare no competing or financial interests.

729

730   **FUNDING**

731   This work was supported by the US National Science Foundation [DBI-1612230 to A.M.O.,

732   IOS-1655756 to E.L.B. and A.L.C., DBI-1661129 to E.L.B., and DGE-1644760 to E.B.K.], the

733   UK Biotechnology and Biological Sciences Research Council [Fellowship BB/ R011109/1 to

734   A.L.C.], and the Bushnell Research and Education Fund [E.B.K., A.M.O.].

735

736   **DATA AVAILABILITY**

737   X-ray video, pressure, and CT data and their essential metadata for this publication have been

738   deposited in the XMAPortal (xmaportal.org), in the study "Knifefish Suction Feeding," with the

739   permanent identifier BROWN65. The data will be publicly available under CCBY 4.0 upon

740   publication in the Public Data Collection "Royal Knifefish data for Li, Kaczmarek et al., 2022"

741   with the full URL:

742   https://xmaportal.org/webportal/larequest.php?request=CollectionView&StudyID=65&instit=BR

743   OWN&collectionID=22

REFERENCES

Altringham, J. D., Wardle, C. S. and Smith, C. I. (1993). Myotomal muscle function at different locations in the body of a swimming fish. *J. Exp. Biol.* **182**, 191–206.

Askew, G. N. and Marsh, R. L. (2001). The mechanical power output of the pectoralis muscle of blue-breasted quail (*Coturnix chinensis*): the in vivo length cycle and its implications for muscle performance. *J. Exp. Biol.* **204**, 3587–3600.

Astley, H. C. and Roberts, T. J. (2012). Evidence for a vertebrate catapult: elastic energy storage in the plantaris tendon during frog jumping. *Biol. Lett.* **8**, 386–389. doi:10.1098/rsbl.2011.0982

Astley, H. C., Abbott, E. M., Azizi, E., Marsh, R. L., Roberts, T. J. (2013). Chasing maximal performance: a cautionary tale from the celebrated jumping frogs of Calaveras County. *J. Exp. Biol.* **216**, 3947-3953. doi:10.1242/jeb.090357.

Brainerd, E. L., Baier, D. B., Gatesy, S. M., Hedrick, T. L., Metzger, K. A., Gilbert, S. L. and Crisco, J. J. (2010). X-ray reconstruction of moving morphology (XROMM): precision, accuracy and applications in comparative biomechanics research. *J. Exp. Zool. Part A Ecol. Genet. Physiol.* **313A**, 262–279. doi:10.1002/jez.589

Brainerd, E. L., Blob, R. W., Hedrick, T. L., Creamer, A. T. and Müller, U. K. (2017). Data management rubric for video data in organismal biology. *Integr. Comp. Biol.* **57**, 33–47. doi:10.1093/icb/icx060

Camp, A. L. (2021). A neck-like vertebral motion in fish. *Proc. R. Soc. B* **288**, 20211091. doi:10.1098/rspb.2021.1091

Camp, A. L. and Brainerd, E. L. (2014). Role of axial muscles in powering mouth expansion during suction feeding in largemouth bass (*Micropterus salmoides*). *J. Exp. Biol.* **217**, 1333–1345. doi:10.1242/jeb.095810

Camp, A. L. and Brainerd, E. L. 2022. A new conceptual framework for the musculoskeletal biomechanics and physiology of ray-finned fishes. *J. Exp. Biol.* **225** (Suppl_1): jeb243376. doi:10.1242/jeb.243376

Camp, A. L., Roberts, T. J. and Brainerd, E. L. (2015). Swimming muscles power suction feeding in largemouth bass. *Proc. Natl. Acad. Sci.* **112**, 8690–8695. doi:10.1073/pnas.1508055112

774   **Camp, A. L., Astley, H. C., Horner, A. M., Roberts, T. J. and Brainerd, E. L.** (2016).

775   Fluoromicrometry: A method for measuring muscle length dynamics with biplanar

776   videofluoroscopy. *J. Exp. Zool.* **325A**, 399–408. doi:10.1002/jez.2031

777   **Camp, A. L., Roberts, T. J. and Brainerd, E. L.** (2018). Bluegill sunfish use high power

778   outputs from axial muscles to generate powerful suction-feeding strikes. *J. Exp. Biol.*

779   **221**. doi:10.1242/jeb.178160

780   **Camp, A. L., Olsen, A. M., Patricia Hernandez, L. and Brainerd, E. L.** (2020). Fishes

781   can use axial muscles as anchors or motors for powerful suction feeding. *J. Exp. Biol.*

782   **223**. doi:10.1242/jeb.225649

783   **Carroll, A. M.** (2004). Muscle activation and strain during suction feeding in the

784   largemouth bass *Micropterus salmoides*. *J. Exp. Biol.* **207**, 983–991.

785   doi:10.1242/jeb.00862

786   **Carroll, A. M. and Wainwright, P. C.** (2009). Energetic limitations on suction feeding

787   performance in centrarchid fishes. *J. Exp. Biol.* **212**, 3241–3251.

788   doi:10.1242/jeb.033092

789   **Carroll, A. M., Wainwright, P. C., Huskey, S. H., Collar, D. C. and Turingan, R. G.**

790   (2004). Morphology predicts suction feeding performance in centrarchid fishes. *J. Exp.*

791   *Biol.* **207**, 3873–3881. doi:10.1242/jeb.01227

792   **Carroll, A. M., Ambrose, A. M., Anderson, T. A. and Coughlin, D. J.** (2009). Feeding

793   muscles scale differently from swimming muscles in sunfish (Centrarchidae). *Biol.*

794   *Lett.* **5**, 274–277. doi:10.1098/rsbl.2008.0647

795   **Coombs, S. and Popper, A. N.** (1982). Structure and function of the auditory system in the

796   clown knifefish, *Notopterus chitala*. *J. Exp. Biol.* **97**, 225–239.

797   doi:10.1242/jeb.97.1.225

798   **Coughlin, D. J. and Carroll, A. M.** (2006). In vitro estimates of power output by epaxial

799   muscle during feeding in largemouth bass. *Comp. Biochem. Physiol. Part A Mol.*

800   *Integr. Physiol.* **145**, 533–539. doi:10.1016/j.cbpa.2006.08.026

801   **Curtin, N. A., Woledge, R. C. and Aerts, P.** (2005). Muscle directly meets the vast power

802   demands in agile lizards. *Proc. R. Soc. B* **272**, 581–584. doi:10.1098/rspb.2004.2982

803   **Edelsbrunner, H., Kirkpatrick, D. and Seidel, R.** (1983). On the shape of a set of points

804   in the plane. *IEEE Trans. Inf. Theory.* **29**, 551-559. doi:10.1109/tit.1983.1056714

805   **Gidmark, N. J., Staab, K. L., Brainerd, E. L. and Hernandez, L. P.** (2012). Flexibility

806   in starting posture drives flexibility in kinematic behavior of the kinethmoid-mediated

807   premaxillary protrusion mechanism in a cyprinid fish, *Cyprinus carpio*. *J. Exp. Biol.*

808   **215**, 2262–2272. doi:10.1242/jeb.070516

809   **Higham, T. E., Day, S. W. and Wainwright, P. C.** (2006). The pressures of suction

810   feeding: the relation between buccal pressure and induced fluid speed in centrarchid

811   fishes. *J. Exp. Biol.* **209**, 3281-7. doi:10.1242/jeb.02383

812   **Jimenez, Y. E. and Brainerd, E. L.** (2020). Dual function of epaxial musculature for

813   swimming and suction feeding in largemouth bass. *Proc. R. Soc. B* **287**.

814   doi:10.1098/rspb.2019.2631

815   **Jimenez, Y. E. and Brainerd, E. L.** (2021). Motor control in the epaxial musculature of

816   bluegill sunfish in feeding and locomotion. *J. Exp. Biol.* **224**. doi:10.1242/jeb.242903

817   **Jimenez, Y. E., Camp, A. L., Grindall, J. D. and Brainerd, E. L.** (2018). Axial

818   morphology and 3D neurocranial kinematics in suction-feeding fishes. *Biol. Open* **7**.

819   doi:10.1242/bio.036335

820   **Jimenez, Y. E., Marsh, R. L. and Brainerd, E. L.** (2021). A biomechanical paradox in

821   fish: swimming and suction feeding produce orthogonal strain gradients in the axial

822   musculature. *Sci. Rep.* **11**, 1–9. doi:10.1038/s41598-021-88828-x

823   **Knörlein, B. J., Baier, D. B., Gatesy, S. M., Laurence-Chasen, J. D. and Brainerd, E.**

824   **L.** (2016). Validation of XMALab software for marker-based XROMM. *J. Exp. Biol.*

825   **219**, 3701–3711. doi:10.1242/jeb.145383

826   **Lauder, G. V and Liem, K. F.** (1981). Prey capture by *Luciocephalus pulcher*:

827   implications for models of jaw protrusion in teleost fishes. *Environ. Biol. Fishes* **6**,

828   257–268.

829   **Liem, K. F.** (1967). Functional morphology of the head of the anabantoid teleost fish

830   *Helostoma temmincki*. *J. Morphol.* **121**, 135–157. doi:10.1002/jmor.1051210204

831   **Lomax, J. J., Martinson, T. F., Jimenez, Y. E. and Brainerd, E. L.** (2020). Bifunctional

832   role of the sternohyoideus muscle during suction feeding in striped surfperch,

833   *Embiotoca lateralis*. *Integr. Org. Biol.* **2**. doi:10.1093/iob/obaa021

834   **Longo, S. J., McGee, M. D., Oufiero, C. E., Waltzek, T. B. and Wainwright, P. C.**

835   (2016). Body ram, not suction, is the primary axis of suction-feeding diversity in

836   spiny-rayed fishes. *J. Exp. Biol.* **219**, 119–128. doi:10.1242/jeb.129015

837   **Muller, M., Osse, J. W. M. and Verhagen, J. H. G.** (1982). A quantitative

838   hydrodynamical model of suction feeding in fish. *J. Theor. Biol.* **95**, 49–79.

839   doi:10.1016/0022-5193(82)90287-9

840   **Norton, S. F. and Brainerd, E. L.** (1993). Convergence in the feeding mechanics of

841   ecomorphologically similar species in the centrarchidae and cichlidae. *J. Exp. Biol.* **29**,

842   11–29. doi:10.1242/jeb.176.1.11

843   **Olsen, A. M., Hernández, L. P., Camp, A. L. and Brainerd, E. L.** (2019). Channel

844   catfish use higher coordination to capture prey than to swallow. *Proc. R. Soc. B* **286**.

845   doi:10.1098/rspb.2019.0507

846   **Osse, J. W. M.** (1969). Functional morphology of the head of the perch (*Perca Fluviatilis*

847   *L.*): an electromyographic study. *Netherlands J. Zool.* **19**, 289–392.

848   doi:10.1163/002829669X00134

849   **Sanford, C. P. J. and Lauder, G. V.** (1989). Functional morphology of the "tongue-bite"

850   in the osteoglossomorph fish *Notopterus*. *J. Morphol.* **202**, 379–408.

851   doi:10.1002/jmor.1052020307

852   **Tegge, S., Hall, J. and Huskey, S.** (2020). Spatial and temporal changes in buccal pressure

853   during prey-capture in the trumpetfish (*Aulostomus maculatus*). *Zoomorphology* **139**,

854   85–95. doi:10.1007/s00435-019-00470-4

855   **Van Wassenbergh, S.** (2015). A solution strategy to include the opening of the opercular

856   slits in moving-mesh CFD models of suction feeding. *Integr. Comp. Biol.* **55**, 62–73.

857   doi:10.1093/icb/icv031

858   **Van Wassenbergh, S., Aerts, P. and Herrel, A.** (2005). Scaling of suction-feeding

859   kinematics and dynamics in the African catfish, *Clarias gariepinus*. *J. Exp. Biol.* **208**,

860   2103–2114. doi:10.1242/jeb.01603

861   **Van Wassenbergh, S., Aerts, P. and Herrel, A**. (2006a). Hydrodynamic modelling of

862   aquatic suction performance and intra-oral pressures: Limitations for comparative

863   studies. *J. R. Soc. Interface.* **3**, 507–514. doi:10.1098/rsif.2005.0110

864   **Van Wassenbergh, S., Aerts, P. and Herrel, A.** (2006b). Scaling of suction feeding

865   performance in the catfish *Clarias gariepinus*. *Physiol. Biochem. Zool.* **79**, 43–56.

866   doi:10.1086/498188

867   **Van Wassenbergh, S., Herrel, A., Adriaens, D. and Aerts, P.** (2007a). Interspecific
868   variation in sternohyoideus muscle morphology in clariid catfishes: functional
869   implications for suction feeding. *J. Morphol.* **268**, 268–242. doi:10.1002/jmor.10510

870   **Van Wassenbergh, S., Herrel, A., James, R. S. and Aerts, P.** (2007b). Scaling of
871   contractile properties of catfish feeding muscles. J. Exp. Biol. **210**, 1183–1193.
872   doi:10.1242/jeb.000109

873   **Van Wassenbergh, S., Strother, J. A., Flammang, B. E., Ferry-Graham, L. A. and**
874   **Aerts, P.** (2008). Extremely fast prey capture in pipefish is powered by elastic recoil.
875   *J. R. Soc. Interface* **5**, 285–296. doi:10.1098/rsif.2007.1124

876   **Van Wassenbergh, S., Dries, B. and Herrel, A.** (2014). New Insights into Muscle
877   Function during Pivot Feeding in Seahorses. *PLoS One* 9, e109068.
878   doi:10.1371/journal.pone.0109068

879   **Van Wassenbergh, S., Day, S. W., Hernández, L. P., Higham, T. E. and Skorczewski,**
880   **T.** (2015). Suction power output and the inertial cost of rotating the neurocranium to
881   generate suction in fish. *J. Theor. Biol.* **372**, 159–167. doi:10.1016/j.jtbi.2015.03.001

882

883

884 **TABLES**

885 **Table 1.** Mean ($\pm$ s.e.m) measurements of peak pressure, change in buccal volume, power, total

886 body mass, bilateral axial and sternohyoid muscle mass, and peak muscle mass-specific power of

887 each individual. Mean peak axial and sternohyoid muscle strain and shortening velocity were

888 measured during the period of peak power.

889

Variable	Cb01 (N = 6)	Cb03 (N = 6)	Cb04 (N = 10)
Peak pressure, kPa	-7.9 ± 2.0	[*] -15.2 ± 4.5	-44.2 ± 3.5
Peak change in buccal volume, cm^3	23.4 ± 3.5	[*] 15.9 ± 2.5	54.2 ± 3.4
Peak rate of volume change, cm^3 s^{-1}	1000 ± 239	[*] 829 ± 178	2518 ± 127
Peak power, W	6.5 ± 2.1	[*] 15.9 ± 6.2	100.6 ± 10.5
Total body mass, g	217	170	480
Epaxial			
[▲] Muscle mass, g	52.7	[**] 44.1	125.2
Initial muscle length, mm	115.1 ± 0.6	109.4 ± 0.5	103.4 ± 0.2
Peak muscle strain, %	3.4 ± 0.4	7.9 ± 1.4	8.0 ± 0.7
Peak muscle velocity, L_i s^{-1}	2.0 ± 0.2	4.6 ± 1.5	4.7 ± 0.1
Hypaxial			
Muscle mass, g	27.5	[**] 25.5	73.7
Initial muscle length, mm	[***] 100.4 ± 3.0	[****] ____	65.3 ± 0.5
Peak muscle strain, %	[***] 1.8 ± 2.8	[****] ____	-1.1 ± 1.3
Peak muscle velocity, L_i s^{-1}	[***] 1.7 ± 0.7	[****] ____	4.1 ± 0.3
Sternohyoid			
Muscle mass, g	2.0	[**] 1.5	4.6
Initial muscle length, mm	21.2 ± 0.07	9.3 ± 0.05	15.3 ± 0.01
Peak muscle strain, %	2.5 ± 0.7	2.5 ± 1.0	2.7 ± 0.4
Peak muscle velocity, L_i s^{-1}	2.7 ± 0.8	4.2 ± 0.9	4.8 ± 0.4
Peak muscle mass-specific power, W kg^{-1}	79.1 ± 25.6	[*] 223.6 ± 87.2	494.3 ± 16.2

[*] Pressure, volume, and power values for Cb03 were measured for N = 7.

[▲] Dorsal column muscle mass is included in the total epaxial muscle masses.

[**] Bilateral muscle mass was estimated for Cb03 because individual was not available for muscle dissection.

[***] Shortening of ventral (anal fin) muscle are reported here because hypaxial beads were not present in Cb01.

[****] Hypaxial values were not recorded because hypaxial beads were not present in Cb03.

890

891 **Table 2.** Comparative measurements for largemouth bass (*Micropterus salmoides*), bluegill
892 sunfish (*Lepomis macrochirus*), channel catfish (*Ictalurus punctatus*), and royal knifefish
893 (*Chitala blanci*). Data shown for royal knifefish are from this study, and data for other species
894 are from previously published datasets (largemouth bass data from Camp et al., 2015; bluegill
895 sunfish data from Camp et al., 2018; and channel catfish data from Camp et al., 2020). Where
896 error values are included, they are the s.e.m (standard error of measurement).
897

Variable	Largemouth Bass	Bluegill Sunfish	Channel Catfish	Royal Knifefish
Across individuals	N = 3	N = 2	N = 3	N = 3
Mean epaxial mass per body mass (%)	17.8 ± 2.9	16.1 ± 0.04	12.5 ± 1.0	25.4 ± 0.6
Mean neurocranial elevation (deg)	[*] 16.0	[*] 12.7	[*] -1.6	[*▲] 24.7
Maximum neurocranial elevation (deg)	[*] 26.0	[*] 17.0	[**] __	[*] 41.0
Mean cleithral retraction (deg)	[*] -9.3	[*] -6.0	[*] -7.7	[*] -2.0
Highest performing individual	Bass02	Bluegill 1	Cat5	Cb04
Body mass (g)	447	164	860	480
[*****] Contributing muscle mass (g)	106.4	42.7	144.22	203.5
Mean peak values of the highest performing individual	N = 9	N = 6	N = 9	N = 10
Pressure (kPa)	-9.7 ± 1.4	-32.2 ± 2.2	-18.4 ± 3.1	-44.2 ± 3.5
Rate of volume change ($cm^3\ s^{-1}$)	882 ± 87	387 ± 58	928 ± 70	2518 ± 127
Power (W)	7.9 ± 1.4	11.4 ± 2.1	13.9 ± 2.9	100.6 ± 10.5
Body mass-specific power ($W\ kg^{-1}$)	17.7 ± 3.1	69.5 ± 12.8	16.2 ± 3.4	209.6 ± 21.9
Muscle mass-specific power ($W\ kg^{-1}$)	74.2 ± 13.2	267.0 ± 49.2	96.4 ± 20.1	494.3 ± 51.6
Body mass-specific rate of volume change ($cm^3\ s^{-1}\ g^{-1}$)	2.0 ± 0.2	2.4 ± 0.4	1.1 ± 0.1	5.2 ± 0.3
Epaxial strain (% L_i)	[***] 4.6 ± 0.3	3.9 ± 0.5	-0.4 ± 0.7	[▲]8.0 ± 0.7
Epaxial shortening velocity ($L_i\ s^{-1}$)	[***] 1.2 ± 0.2	[▲]2.2 ± 0.3	[▲] 0.1 ± 0.04	[▲] 4.7 ± 0.1
Hypaxial strain (%L_i)	[***] 8.4 ± 1.7	6.8 ± 0.6	8.3 ± 2.4	[▲]-1.1 ± 1.3; [****▲]3.0 ± 0.3
Hypaxial shortening velocity ($L_i\ s^{-1}$)	[***] 1.6 ± 0.6	[▲]3.4 ± 0.2	[▲]1.3 ± 0.1	[▲]4.1 ± 0.3

[*]Positive values for neurocranial and cleithral rotation represent elevation, while negative values represent retraction.

[**]Maximum neurocranium elevation for channel catfish was not reported because neurocranium consistently depressed rather than elevated.

[▲] Measurements were made during the period of peak power rather than the maximum recorded value during the strike.

[***] For axial muscle strain N = 10, and for axial muscle shortening velocity N = 6.

[****] Hypaxial strain was measured with L_i defined at the start of shortening rather than the start of the strike.

[*****] Contributing muscle mass only includes the mass of axial muscle that shortened and the sternohyoid if it shortened (all species but largemouth bass).

898

899 **FIGURE LEGENDS**

900 **Fig. 1. Body shape and anatomy of the axial musculature and skeleton in royal knifefish,**

901 *Chitala blanci***, compared with the body shapes of three other species for which suction**

902 **power has been measured.** (A) Lateral view of the neurocranium, cleithrum, and left-side bones

903 of the head in *C. blanci*. Dashed line indicates the approximate location of the cross-section

904 shown in (B). (B) Transverse cross-section of *C. blanci*, illustrating its inverted teardrop shape.

905 (C) Whole-body shape and (D) transverse cross-section comparisons of *C. blanci* to other

906 previously studied species: channel catfish (*Ictalurus punctatus*), bluegill sunfish (*Lepomis*

907 *macrochirus*), and largemouth bass (*Micropterus salmoides*). Fishes are shown with expanded

908 mouths in (C).

909
910 **Fig. 2. Sample XROMM animation and measurement of buccal cavity volume before and**

911 **during suction expansion.** Animated bone models before suction expansion (A,C,E) and during

912 suction expansion (B,D,F). (A,B) Right lateral view of X-ray image with animated

913 neurocranium, left cleithrum, and left-side bone meshes. Surgically implanted bone and

914 intramuscular (epaxial, hypaxial, dorsal column, and sternohyoid) markers are visible as black

915 circles. (C,D) Left lateral view of animated bone models and (E,F) animated dynamic endocast

916 of buccal cavity volume.

917
918 **Fig. 3. Buccal volume, rate of volume change, intraoral pressure, and suction power in the**

919 **highest power strike.** (A) Buccal volume, measured using dynamic endocast. (B) Rate of

920 volume change (black, left axis) and intraoral pressure relative to ambient pressure (blue, right

921 axis). (C) Suction power was calculated as the product of intraoral pressure and rate of volume

922 change at each time point. Peak suction power (within 25% of maximum) is indicated by the

923 shaded region with the corresponding values highlighted in red.

924

Fig. 4. Suction power (W) and muscle mass-specific power (W kg^{-1}) in three royal knifefish. Absolute suction power (left y-axis) is plotted relative to peak gape for each strike in each individual. The right y-axis shows muscle mass-specific power, which divides suction power by the combined mass of the epaxial and hypaxial shortening regions and the sternohyoid.

Fig. 5. Neurocranium and cleithrum rotations relative to the body plane and muscle length changes during buccal expansion in royal knifefish. Data from each individual are shown separately, with the period of peak power (within 25% of maximum) highlighted in red and the time of peak power marked with a red dot. (A) Z-axis rotation (relative to initial values) of the neurocranium (row 1) and left cleithrum (row 2) relative to the body plane. Positive values represent elevation or protraction (white region), while negative values represent depression or retraction (shaded region). (B) For each muscle (bottom three rows), muscle length was normalized by its mean initial length (L_i). Values below 1 (shaded region) represent shortened muscle, while those greater than 1 (white region) represent lengthened muscle relative to L_i.

Fig. 6. Maximum epaxial and hypaxial muscle strain along the body. (A) Epaxial strain and (B) ventral (anal fin) muscle and hypaxial strain during the period of peak power were calculated as percent change in length relative to the mean initial length (L_i) in subregions along the cranial half of the body. Maximum strain for each strike (red or blue circles) and mean strain (red or blue bars) across all strikes are shown for each subregion with positive values representing muscle shortening. The width of the bar reflects the craniocaudal length of each muscle subregion. Note that Cb03 did not have ventral or hypaxial strain data.
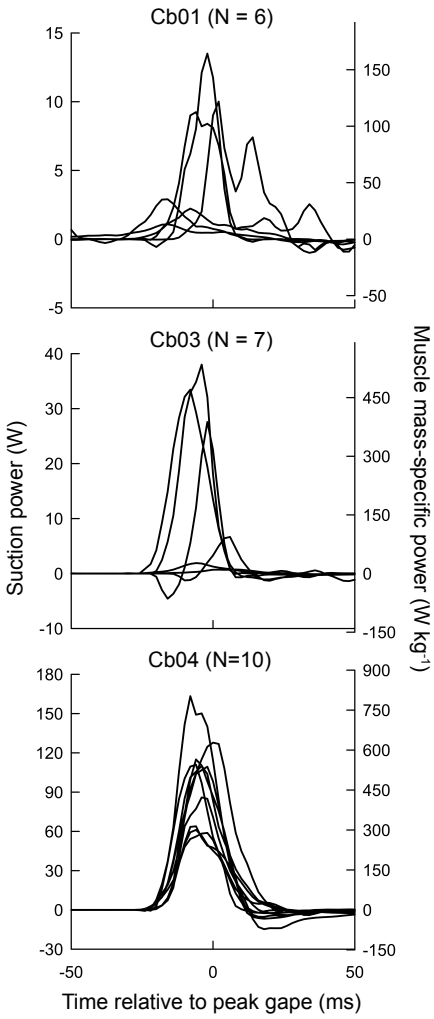
Fig. 7. Comparison of suction power of royal knifefish to three other species. Data are shown for royal knifefish (n = 23 strikes, from this study), channel catfish (n = 24 strikes, data from Camp et al., 2020), largemouth bass (n = 29 strikes, data from Camp et al., 2015), and bluegill sunfish (n = 11 strikes, data from Camp et al., 2018). Power per strike (colored circles) and average power across all strikes from each individual (black circles) are shown. For all species, suction power was calculated as (A) the absolute magnitude of maximum suction power, (B) maximum suction power relative to the total body mass of the individual, and (C) maximum suction power relative to the maximum change in buccal volume for each strike.

A

Dorsal column of muscle
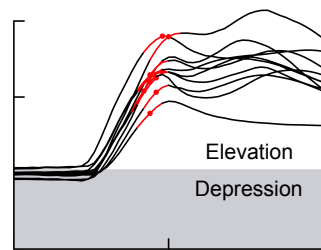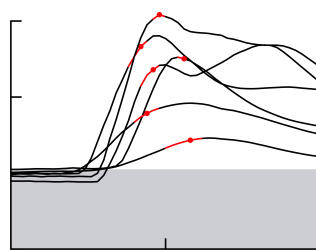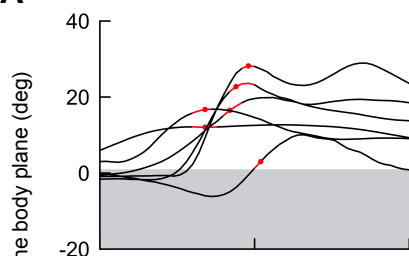
Epaxial muscle

Neurocranium

Cleithrum · Hypaxial muscle · Anal fin muscle

B

Dorsal column of muscle

Epaxial muscle

Hypaxial muscle

C

Royal knifefish

Channel catfish

Bluegill sunfish

Largemouth bass

D

Cb01 (N = 6)

Cb03 (N = 7)

Cb04 (N=10)

Suction power (W)
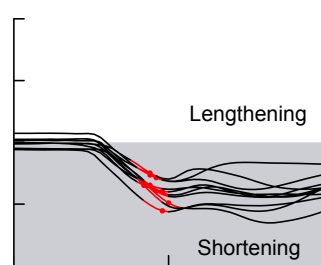
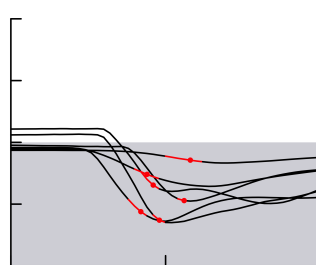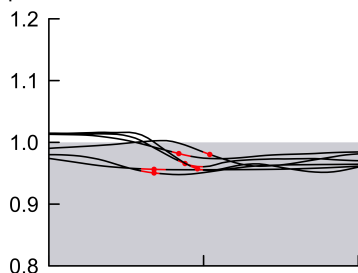Muscle mass-specific power (W kg^{-1})
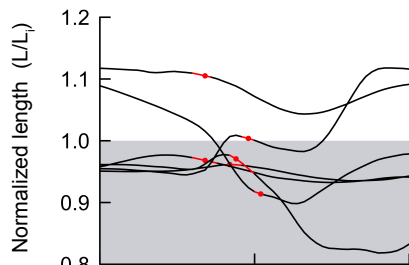
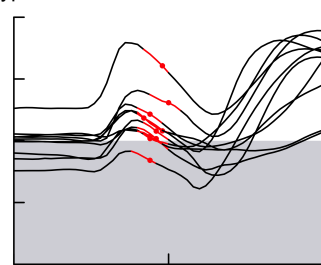Time relative to peak gape (ms)
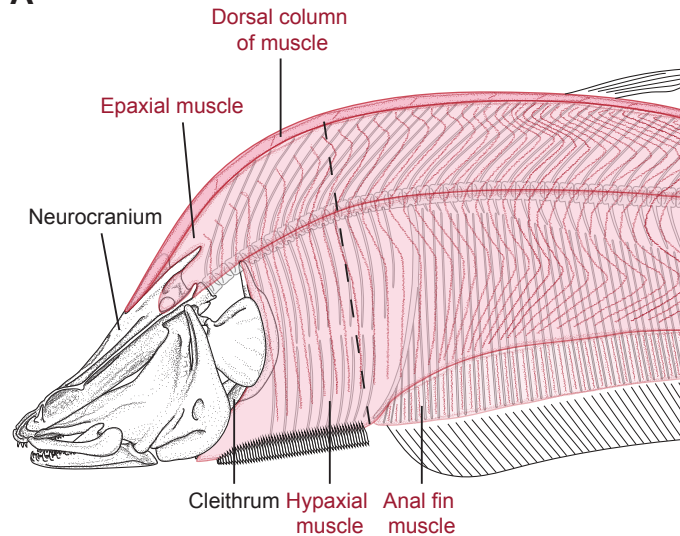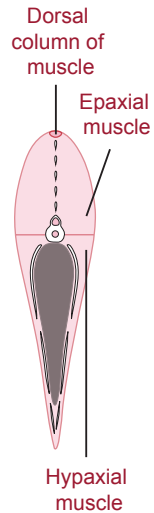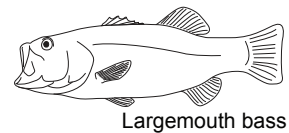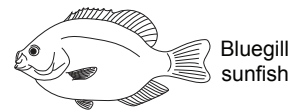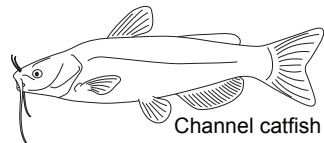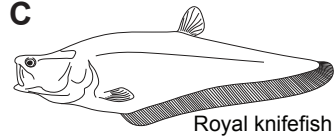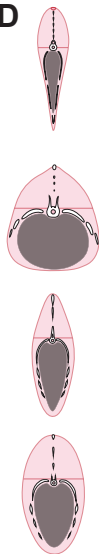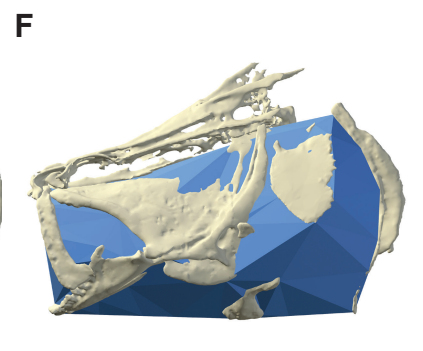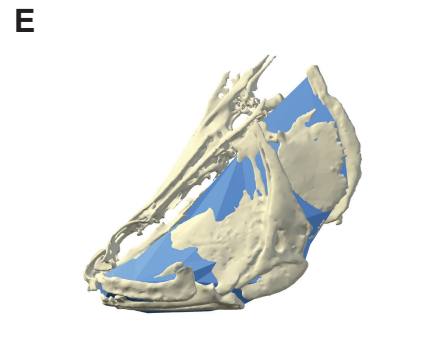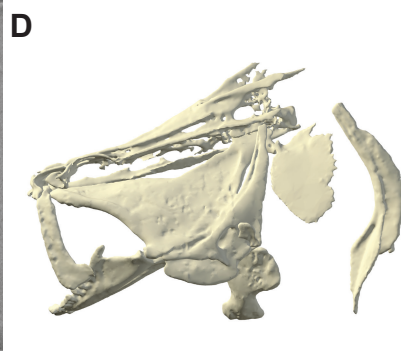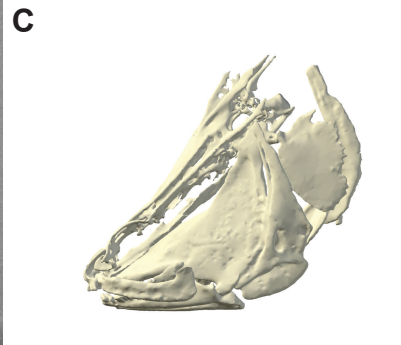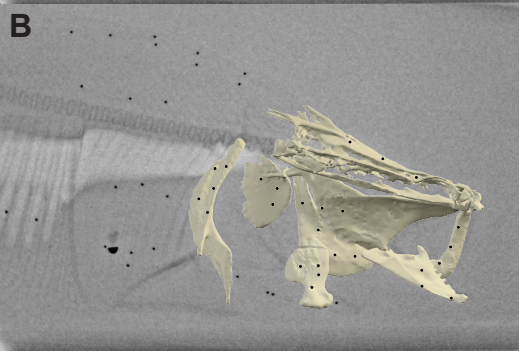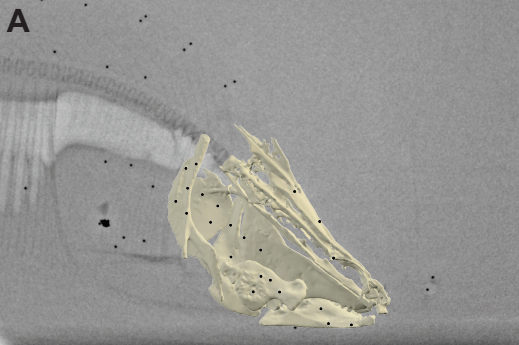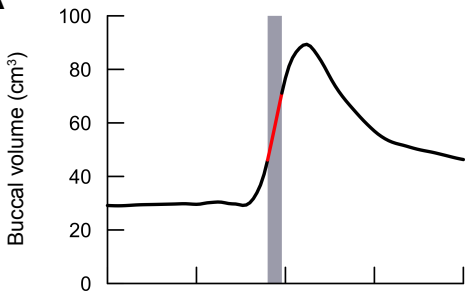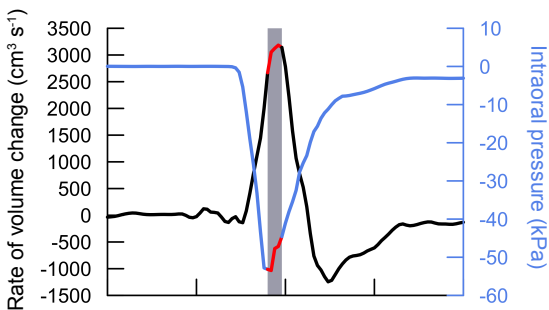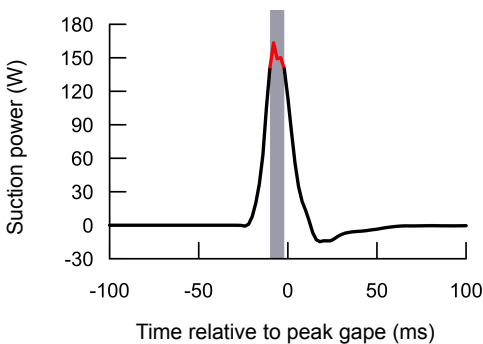
Cb01 (N=6) Cb03 (N=6) Cb04 (N=10)

A Neurocranium

Cleithrum
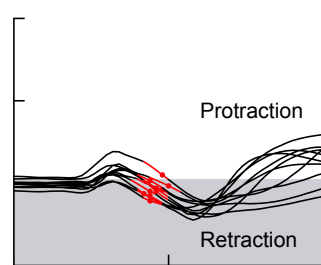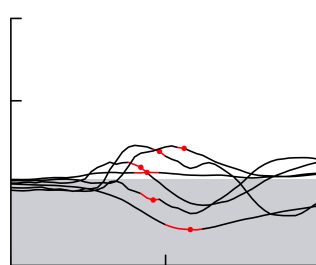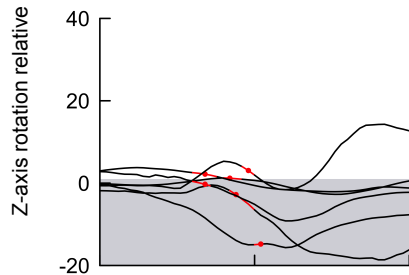
B Epaxial
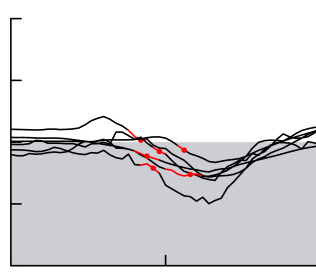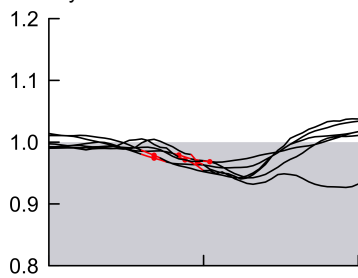
Ventral muscle Hypaxial

Sternohyoid

Z-axis rotation relative to the body plane (deg)

Normalized length (L/L_i)

Time relative to peak gape (ms)

Elevation / Depression

Protraction / Retraction

Lengthening / Shortening

A

Cb01
N = 6 strikes
Epaxial

Cb03
N = 6 strikes
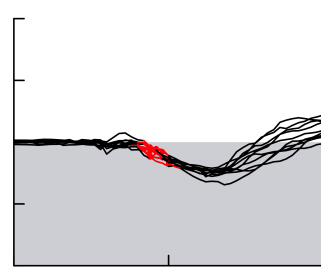
Cb04
N = 10 strikes

Maximum strain during period of peak power (%L_L)

Muscle subregions

B

Ventral Muscle

Cb01
N = 6 strikes

Hypaxial

Cb04
N = 10 strikes

Muscle subregions

A

Absolute suction power (W)

B

Body mass-specific power (W kg^{-1})

C

Volume-specific power (W cm^{-3})

Individuals

Royal
knifefish

Channel
catfish

Largemouth
bass

Bluegill
sunfish